Comput Mech
DOI 10.1007/s00466-015-1191-9

ORIGINAL PAPER

Modeling and simulation of cooling-induced residual stresses in heated particulate mixture depositions in additive manufacturing

T. I. Zohdi[1]

Received: 10 April 2015 / Accepted: 27 July 2015

Abstract One key aspect of many additive manufacturing processes is the deposition of heated mixtures of particulate materials onto surfaces, which then bond and cool, leading to complex microstructures and possible residual stresses. The overall objective of this work is to construct a straightforward computational approach that researchers in the field can easily implement and use as a numerically-efficient simulation and design tool. Specifically because multifield coupling is present, a recursive, staggered, temporally-adaptive, finite difference time domain scheme is developed to resolve the internal microstructural thermal and mechanical fields, accounting for the simultaneous elasto-plasticity and damage. The time step adaptation allows the numerical scheme to iteratively resolve the changing physical fields by refining the time-steps during phases of the process when the system is undergoing large changes on a relatively small time-scale and can also enlarge the time-steps when the processes are relatively slow. The spatial discretization grids are uniform and dense. The deposited microstructure is embedded into spatial discretization. The regular grid allows one to generate a matrix-free iterative formulation which is amenable to rapid computation and minimal memory requirements, making it ideal for laptop computation. Numerical examples are provided to illustrate the approach. This formulation is useful for material scientists who seek ways to deposit such materials while simultaneously avoiding inadvertent excessive residual stresses.

Keywords Particulates · Multiphysics · Residual stresses

✉ T. I. Zohdi
zohdi@me.berkeley.edu

[1] Department of Mechanical Engineering, University of California, 6195 Etcheverry Hall, Berkeley, CA 94720-1740, USA

1 Introduction to additive processes

1.1 Motivation

The use of deposited particulate mixtures of materials has recently become of high interest to industry because of the rise of Additive Manufacturing (AM), Rapid-Prototyping and 3D printing (Fig. 1). Today, large quantities of inexpensive, high-quality, particles for manufacturing processes, are readily available due to advanced materials processing techniques such as (a) sublimation from a raw solid to a gas, which condenses into particles that are recaptured (harvested), (b) atomization of liquid streams into droplets by breaking jets of metal, (c) reduction of metal oxides and (d) precise comminution/pulverizing of bulk material.

In 2014, print-like based technologies employing deposition of particulate materials, spanning metals to plastics, and in some cases biological and organic materials was a 2.2 billion dollar industry.[1] Applications range from commercial manufacturing, military, academia, medical to the arts, with a rough market breakdown being 30 % motor vehicles, 15 % consumer products, medical 9 % and business 11 %. For an early history of the printed electronics field, see Gamota et al. [24]. For reviews of related optical coatings and photonics, see Nakanishi et al. [54], for catalysts, see Haruta [29] and for MEMS applications, see Fuller et al. [23]. AM methods involving particles are, in theory, ideal for large-surface area applications. These types of applications and associated technology are closely related to those in the area spray coatings, and we refer the reader to the extensive works of Sevostianov and Kachanov [68–70] and to Nakamura and coworkers: Dwivedi et al. [21], Liu et al. [47,48], Nakamura

[1] 3D printing was pioneered by Hull [33] of the 3D-Systems Corporation in 1984.

Published online: 23 August 2015

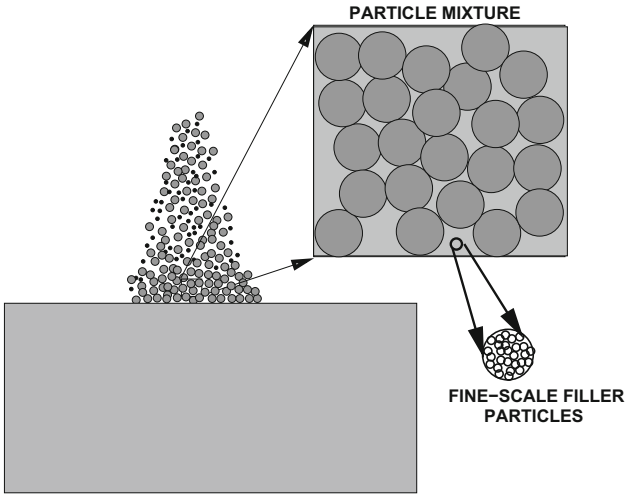

Fig. 1 Hot deposited particle mixtures on a surface

and Liu [52], Nakamura et al [53] and Qian et al [59]. For a general review of deposition and spray technology, see Martin [40,41].

1.2 Objectives

This work is concerned with the computational characterization of the evolution of residual stresses in materials with microstructures that arise from deposited hot mixtures of particles which cool down. Residual stresses arise because the hot bonded materials cannot freely contract to their stress-free state, due to to their interaction with other components in the system and the surrounding environment to which they are bonded.[2] The objective of this work is to develop a straightforward computational framework that researchers in the field can easily implement and use as a computationally-efficient design tool. Generally speaking, there is thermo-mechanical multifield coupling present, along with material changes associated with material hardening, elasto-plasticity and mechanical damage. Specifically, a recursively staggered, temporally-adaptive, finite difference time domain (FDTD) scheme is developed to resolve the internal microstructural thermal and mechanical fields, accounting for the simultaneous elasto-plasticity and damage. The time step adaptation is constructed to allow the numerical scheme to iteratively resolve the changing physical fields by reducing the time-steps during phases of the process when the system is undergoing changes on relatively small time-scales and also to enlarge the time-steps when the processes are relatively slow. The spatial discretization grids are uniform and dense, with the complex microstructure being embedded into the mesh. The regular grid allows one to generate a matrix-free iterative formulation which is amenable to rapid computation and minimal memory requirements, making it ideal for laptop computation. The presentation is broken into three main parts: (1) formulations for each field in the model problem, identifying the coupling terms, (2) iterative staggering schemes (including spatial and temporal discretization) and (3) numerical examples for the model problem. The approach builds on work found in Zohdi [79,81,82,85] and [88] and then applies it to particle mixture deposition systems.

Remarks In this work, we focus on the cooling of a hot particulate mixture. The initial dynamic deposition process of multibody and inter-particle collisions is outside the scope of the present work. However, we mention in passing that to model the dynamics of particle systems, reduced-order particle-based or discrete element-based models, which treat such systems as multibody dynamical groups, are often used. They are advantageous in dealing with domains that break apart or coalesce, as compared to traditional continuum based finite difference and finite element methods, which have limitations when dealing with dynamic discontinua. For reviews see, for example, Duran [20], Pöschel and Schwager [58], Onate et al. [56,57], Rojek et al. [62], Carbonell et al. [12], Labra and Onate [42], Leonardi et al [43], Cante et al [11], Rojek [63], Onate et al [64], Bolintineanu et al [7], Campello and Zohdi [9,10], Avci and Wriggers [1] and Zohdi [86,88,91]. In many cases, the deposition of these materials is the first stage of a multistep process which may involve, among other processes, compaction. Compaction is also somewhat outside the scope of the present work, and we refer the reader to Akisanya et al. [2], Anand and Gu [4], Brown and Abou-Chedid [8], Domas [14], Fleck [22], Gethin et al., [25], Gu et al. [28], Lewis et al. [44], Ransing et al. [60], Tatzel [71] and Zohdi [80,81].

2 Transient thermo-mechanical coupled fields

We consider a model problem of a deposited set of hot particles which are in the cool-down phase of the process. The essential field equations and simplifying assumptions that will be used during the analysis are provided next.

2.1 Balance of linear momentum

We consider a balance of linear momentum governed by

$$\nabla_x \cdot \boldsymbol{\sigma} + \boldsymbol{f} = \rho \frac{d^2 \boldsymbol{u}}{dt^2}, \tag{2.1}$$

in regimes where *infinitesimal deformations are appropriate*, where $\boldsymbol{\sigma}$ is the Cauchy stress, $\boldsymbol{f}$ are body forces, ρ is

[2] In many processes, the mixture of particles are heated during deposition to enhance bonding or to decrease the viscosity of the flow through the dispenser. This is essentially a material similar to a functionalized ink or slurry, which may not necessarily involve selective laser processing afterwards.

the material density and $\boldsymbol{u}$ is the displacement. Consistent with the infinitesimal deformation approximation we write $\nabla_x \approx \nabla_X$ and $\frac{d()}{dt} \approx \frac{\partial()}{\partial t}|_X$, where $\boldsymbol{X}$ are the referential coordinates, $\boldsymbol{x}$ are the current coordinates. We consider a constitutive law that describes the evolution of isotropic damage, elasto-plasticity, given by

$$\boldsymbol{\sigma} = \mathcal{D}\mathbb{E}_0 : (\boldsymbol{\epsilon} - \boldsymbol{\epsilon}_\theta - \boldsymbol{\epsilon}_p), \tag{2.2}$$

which under infinitesimal deformation framework the balance of linear momentum becomes ($\rho \approx \rho_o$)

$$\nabla_x \cdot (\mathcal{D}\mathbb{E}_0 : (\boldsymbol{\epsilon} - \boldsymbol{\epsilon}_\theta - \boldsymbol{\epsilon}_p)) + \boldsymbol{f} = \rho \frac{\partial^2 \boldsymbol{u}}{\partial t^2} \tag{2.3}$$

with infinitesimal strains given by $\boldsymbol{\epsilon} = \frac{1}{2}\left(\nabla_x \boldsymbol{u} + (\nabla_x \boldsymbol{u})^T\right)$, thermal strains given by $\boldsymbol{\epsilon}_\theta \overset{\text{def}}{=} \boldsymbol{\gamma} \cdot (\theta - \theta_0)\mathbf{1}$ and plastic strains given by $\boldsymbol{\epsilon}_p$, generated by the following unilateral conditions

$$||\boldsymbol{\sigma}'|| > \sigma_y \Rightarrow \dot{\zeta} = a\left(\frac{||\boldsymbol{\sigma}'||}{\sigma_y} - 1\right) \tag{2.4}$$

and

$$||\boldsymbol{\sigma}'|| \leq \sigma_y \Rightarrow \dot{\zeta} = 0 \tag{2.5}$$

where $\dot{\boldsymbol{\epsilon}}_p = \dot{\zeta}\frac{\boldsymbol{\sigma}'}{||\boldsymbol{\sigma}'||}$ and $\boldsymbol{\sigma}' = \boldsymbol{\sigma} - \frac{tr\boldsymbol{\sigma}}{3}\mathbf{1}$ is the deviatoric stress. Here, the (isotropic) damaged elasticity tensor is $\mathbb{E} = \mathcal{D}\mathbb{E}_0$, where $\mathbb{E}_0$ represents the "virgin" isotropic undamaged material, $0 \leq \mathcal{D} \leq 1$ is the scalar continuity (isotropic damage) parameter (Kachanov [35]), $\mathcal{D}(t = 0) = 1$ indicates the initial undamaged state and $\mathcal{D} \to 0$ indicates a completely damaged state. The damage arising from mechanical sources is modeled as being governed by evolution over-stress functions of the form ($0 < \mathcal{D} \leq 1$)

$$||\boldsymbol{\sigma}'|| > \sigma_d \Rightarrow \dot{\mathcal{D}} = b\left(\frac{||\boldsymbol{\sigma}'||}{\sigma_d} - 1\right) \tag{2.6}$$

and

$$||\boldsymbol{\sigma}'|| \leq \sigma_d \Rightarrow \dot{\mathcal{D}} = 0, \tag{2.7}$$

We note that the rate constants a and b and the critical stresses σ_y and σ_d are potentially spatially-variable. Clearly, further evolution laws can be written for other material property changes, such as the thermal conductivity, although only changes in the mechanical property $\mathbb{E}$ are considered during the formulations to follow.[3] In the case of material isotropy

$$\boldsymbol{\sigma} = \mathcal{D}\left(\lambda_0 tr(\boldsymbol{\epsilon} - \boldsymbol{\epsilon}_\theta - \boldsymbol{\epsilon}_p)\mathbf{1} + 2\mu_0(\boldsymbol{\epsilon} - \boldsymbol{\epsilon}_\theta - \boldsymbol{\epsilon}_p)\right), \tag{2.8}$$

[3] For further details on these types of phenomenological (damage) formulations, the interested reader is referred to the seminal work of Kachanov [35].

where λ_0 is the undamaged Lame parameter and μ_0 is the undamaged shear modulus.

2.2 Balance of energy

The interconversions of various forms of energy (mechanical, thermal, etc) in a system are governed by the first law of thermodynamics,

$$\rho\dot{w} - \boldsymbol{\sigma} : \nabla_x \dot{\boldsymbol{u}} + \nabla_x \cdot \boldsymbol{q} - \rho z = 0, \tag{2.9}$$

where w is the stored energy per unit mass (which is a function of the temperature, θ and elastic strain, $\boldsymbol{\epsilon}^e = \boldsymbol{\epsilon} - \boldsymbol{\epsilon}_\theta - \boldsymbol{\epsilon}_p$), $\boldsymbol{q}$ is heat flux, and ρz is the rate of energy absorbed from sources. We employ the following for the stored energy (assuming infinitesimal deformations)

$$\rho w = W \approx \tfrac{1}{2}(\boldsymbol{\epsilon} - \boldsymbol{\epsilon}_\theta - \boldsymbol{\epsilon}_p) : \mathbb{E} : (\boldsymbol{\epsilon} - \boldsymbol{\epsilon}_\theta - \boldsymbol{\epsilon}_p) + \rho C\theta, \tag{2.10}$$

which implies

$$\begin{aligned}\rho\dot{w} = \dot{W} = (\dot{\boldsymbol{\epsilon}} - \dot{\boldsymbol{\epsilon}}_\theta - \dot{\boldsymbol{\epsilon}}_p) : \mathbb{E} : (\boldsymbol{\epsilon} - \boldsymbol{\epsilon}_\theta - \boldsymbol{\epsilon}_p) \\ + \frac{1}{2}(\boldsymbol{\epsilon} - \boldsymbol{\epsilon}_\theta - \boldsymbol{\epsilon}_p) : \dot{\mathbb{E}} : (\boldsymbol{\epsilon} - \boldsymbol{\epsilon}_\theta - \boldsymbol{\epsilon}_p) + \rho C\dot{\theta},\end{aligned} \tag{2.11}$$

and thus the first law becomes

$$\begin{aligned}\rho C\dot{\theta} = \boldsymbol{\sigma} : (\dot{\boldsymbol{\epsilon}}_\theta + \dot{\boldsymbol{\epsilon}}_p) - \frac{1}{2}(\boldsymbol{\epsilon} - \boldsymbol{\epsilon}_\theta - \boldsymbol{\epsilon}_p) : \dot{\mathbb{E}} : (\boldsymbol{\epsilon} - \boldsymbol{\epsilon}_\theta - \boldsymbol{\epsilon}_p) \\ + \nabla_x \cdot (\mathbb{K} \cdot \nabla_x \theta) + \rho z\end{aligned} \tag{2.12}$$

where Fourier's law, $\boldsymbol{q} = -\mathbb{K} \cdot \nabla_x \theta$, has been used.

3 Iterative staggering scheme

We now develop a staggering solution framework to solve the coupled systems of interest. The general methodology is as follows (at at given time increment): (1) each field equation is solved individually, "freezing" the other (coupled) fields in the system, allowing only the primary field to be active and (2) after the solution of each field equation, the primary field variable is updated, and the next field equation is treated in a similar manner. For an "implicit" type of staggering, the process can be repeated in an iterative manner, while for an "explicit" type, one moves to the next time step after one "pass" through the system. We will employ implicit staggering. Specifically, for the thermo-mechanical system under consideration, consider an abstract setting, whereby one solves for the mechanical field, assuming the thermal

field is fixed (L is a time-step counter and K is a staggering-step counter),

$$\mathcal{A}_1\left(\underline{\boldsymbol{u}}^{L+1,K},\theta^{L+1,K-1}\right)=\mathcal{B}_1\left(\boldsymbol{u}^{L+1,K-1},\theta^{L+1,K-1}\right) \tag{3.1}$$

then one solves for the thermal fields, assuming the mechanical field fixed,

$$\mathcal{A}_2\left(\boldsymbol{u}^{L+1,K},\underline{\theta}^{L+1,K}\right)=\mathcal{B}_2\left(\boldsymbol{u}^{L+1,K},\theta^{L+1,K-1}\right) \tag{3.2}$$

where the only underlined variable is "active" at that stage of the process. Within the staggering (iterative) scheme, implicit time-stepping methods (with time step size adaptivity) will be used throughout the upcoming analysis (described shortly). The process is driven by minimizing nondimensional relative iterative coupling error (of both fields) within a time-step (difference between successive iterations). A tolerance check determines whether the iterations should continue, or if the time steps should be adaptively reduced to increase the rate of convergence. The time steps can be increased if convergence occurs too quickly, thus allowing larger time-steps and faster simulations for a given iterative error tolerance. The details of this process are discussed shortly. Generally speaking, if a recursive staggering process is not employed (an explicit coupling scheme), the staggering error can accumulate rapidly. However, simply employing extremely small time steps, smaller than needed to control the discretization error, in order to suppress a (nonrecursive) staggering process error, can be computationally inefficient. Therefore, the objective of the next subsection is to develop a strategy to adaptively adjust, in fact maximize, the choice of the time step size in order to control the staggering error, while simultaneously staying below a critical time step size needed to control the discretization error. An important related issue is to simultaneously minimize the computational effort involved. We now develop a staggering scheme by extending an approach found in the work of Zohdi [79,81,82,85] and [88].

Remark 1 The symbol $||\cdot||$ will signify the $L_2(\Omega)$-norm throughout this work. The nondimensional error metric for the mechanical field is (where we assume that the denominator is nonzero)

$$\varpi_u^K \stackrel{\text{def}}{=} \frac{\left|\left|\boldsymbol{u}^{L+1,K}-\boldsymbol{u}^{L+1,K-1}\right|\right|}{\left|\left|\boldsymbol{u}^{L+1,K}-\boldsymbol{u}^{L}\right|\right|}, \tag{3.3}$$

and for the thermodynamic field

$$\varpi_\theta^K \stackrel{\text{def}}{=} \frac{\left|\left|\theta^{L+1,K}-\theta^{L+1,K-1}\right|\right|}{\left|\left|\theta^{L+1,K}-\theta^{L}\right|\right|}. \tag{3.4}$$

Thereafter, we select the maximum *nondimensionalized* error for adaptivity

$$\varpi^{*,K} \stackrel{\text{def}}{=} max\left(\varpi_u^K,\varpi_\theta^K\right), \tag{3.5}$$

Remark 2 Staggering schemes are widely used in the computational mechanics literature, dating back, at least, to Zienkiewicz [77] and Zienkiewicz et al. [78]. For in depth overviews, see the works of Lewis and Schrefler (Lewis et al. [45] and Lewis and Schrefler [46]) and a series of works by Schrefler and collaborators: Schrefler [65], Turska and Schrefler [73], Biano et al. [6] and Wang and Schrefler [74].

3.1 Spatial discretization of the fields

Numerically, the components of the gradient of functions such as $\boldsymbol{u}$ and θ are approximated by central finite difference stencils of the basic form (Fig. 9):

$$\frac{\partial u_i}{\partial x_j}|_x \approx \frac{u_i(x_j+\Delta x_j)-u_i(x_j-\Delta x_j)}{2\Delta x_j} \tag{3.6}$$

for each of the (x_1, x_2, x_3)-directions, in order to form the terms needed in $\nabla_x \boldsymbol{u}$ and $\nabla_x \cdot \boldsymbol{\sigma}$. This is a second-order accurate stencil. For a generic second order scheme spatial derivative, such as

$$\frac{\partial \sigma}{\partial x}|_x \approx \frac{\sigma\left(x+\frac{\Delta x}{2}\right)-\sigma\left(x-\frac{\Delta x}{2}\right)}{\Delta x}, \tag{3.7}$$

where generically, for example with an arbitrary material coefficient $a(x)=\lambda(x)$ or $a(x)=\mu(x)$ (Fig. 2):

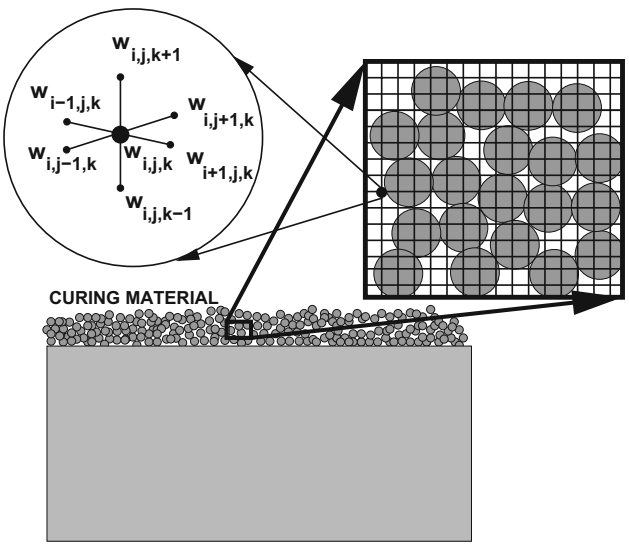

Fig. 2 A typical three dimensional finite-difference stencil for a field $w(x, y, z)$

$$\sigma\left(x+\frac{\Delta x}{2}\right) \approx a\left(x+\frac{\Delta x}{2}\right) \underbrace{\frac{u(x+\Delta x)-u(x)}{\Delta x}}_{\frac{\partial u}{\partial x}|_{x+\frac{\Delta x}{2}}} \tag{3.8}$$

and

$$\sigma\left(x-\frac{\Delta x}{2}\right) \approx a\left(x-\frac{\Delta x}{2}\right) \underbrace{\frac{u(x)-u(x-\Delta x)}{\Delta x}}_{\frac{\partial u}{\partial x}|_{x-\frac{\Delta x}{2}}} \tag{3.9}$$

where

$$a\left(x+\frac{\Delta x}{2}\right) \approx \frac{1}{2}(a(x+\Delta x)+a(x)), \tag{3.10}$$

and

$$a\left(x-\frac{\Delta x}{2}\right) \approx \frac{1}{2}(a(x)+a(x-\Delta x)). \tag{3.11}$$

These approximations are made for all components and combinations in $\nabla_x \cdot \boldsymbol{\sigma}$. The mixed derivatives are derived in a similar manner in Appendix 1. Similarly, for a second order scheme spatial derivatives in the heat conduction

$$\frac{\partial q}{\partial x}|_x \approx \frac{q\left(x+\frac{\Delta x}{2}\right)-q\left(x-\frac{\Delta x}{2}\right)}{\Delta x}, \tag{3.12}$$

where (in conjunction with Fourier's Law)

$$q\left(x+\frac{\Delta x}{2}\right) \approx -\boldsymbol{IK}\left(x+\frac{\Delta x}{2}\right) \underbrace{\frac{\theta(x+\Delta x)-\theta(x)}{\Delta x}}_{\frac{\partial \theta}{\partial x}|_{x+\frac{\Delta x}{2}}} \tag{3.13}$$

and

$$q\left(x-\frac{\Delta x}{2}\right) \approx -\boldsymbol{IK}\left(x-\frac{\Delta x}{2}\right) \underbrace{\frac{\theta(x)-\theta(x-\Delta x)}{\Delta x}}_{\frac{\partial \theta}{\partial x}|_{x-\frac{\Delta x}{2}}} \tag{3.14}$$

where

$$\boldsymbol{IK}\left(x+\frac{\Delta x}{2}\right) \approx \frac{1}{2}(\boldsymbol{IK}(x+\Delta x)+\boldsymbol{IK}(x)), \tag{3.15}$$

and

$$\boldsymbol{IK}\left(x-\frac{\Delta x}{2}\right) \approx \frac{1}{2}(\boldsymbol{IK}(x)+\boldsymbol{IK}(x-\Delta x)). \tag{3.16}$$

These approximations are made for $\frac{\partial q_1}{\partial x_1}$, $\frac{\partial q_2}{\partial x_2}$ and $\frac{\partial q_3}{\partial x_3}$, in order to form the terms needed in $\nabla_x \cdot \boldsymbol{q}$. This is done at each node in the grid. See Appendix 1 for more details.

3.2 Temporal discretization of fields

3.2.1 Mechanical field

For the mechanical field (infinitesimal deformation formulation) we write

$$\frac{d\boldsymbol{v}}{dt} = \frac{\partial \boldsymbol{v}}{\partial t} = \frac{1}{\rho}\left(\nabla_x \cdot \boldsymbol{\sigma} + \boldsymbol{f}\right) \stackrel{\text{def}}{=} \boldsymbol{\Psi}. \tag{3.17}$$

We discretize for time$=t+\phi\Delta t$, and using a trapezoidal "$\phi-scheme$" ($0 \le \phi \le 1$, see Appendix 3)

$$\frac{\boldsymbol{v}(t+\Delta t)-\boldsymbol{v}(t)}{\Delta t} \approx \boldsymbol{\Psi}(t+\phi\Delta t) \approx \phi\boldsymbol{\Psi}(+\Delta t)+(1-\phi)\boldsymbol{\Psi}(t). \tag{3.18}$$

Rearranging, yields

$$\boldsymbol{v}(t+\Delta t) \approx \boldsymbol{v}(t)+\Delta t\left(\phi\boldsymbol{\Psi}(t+\Delta t)+(1-\phi)\boldsymbol{\Psi}(t)\right) \tag{3.19}$$

where the previously introduced spatial discretization is applied to the terms in $\boldsymbol{\Psi}$ ($\nabla_x \cdot \boldsymbol{\sigma}$). Since this is a second-order system, the procedure is then repeated to determine the displacement field $\boldsymbol{u}$ (see Appendix 3)

$$\begin{aligned}\boldsymbol{u}(t+\Delta t) &= \boldsymbol{u}(t)+\boldsymbol{v}(t+\phi\Delta t)\Delta t \\ &= \boldsymbol{u}(t)+\left(\phi\boldsymbol{v}(t+\Delta t)+(1-\phi)\boldsymbol{v}(t)\right)\Delta t,\end{aligned} \tag{3.20}$$

or more explicitly

$$\boldsymbol{u}(t+\Delta t) = \boldsymbol{u}(t)+\boldsymbol{v}(t)\Delta t+\phi(\Delta t)^2\boldsymbol{\Psi}(t+\phi\Delta t). \tag{3.21}$$

The term $\boldsymbol{\Psi}(t+\phi\Delta t)$ can be handled in two main ways:

- $\boldsymbol{\Psi}(t+\phi\Delta t) \approx \boldsymbol{\Psi}(\phi\boldsymbol{u}(t+\Delta t)+(1-\phi)\boldsymbol{u}(t))$ or
- $\boldsymbol{\Psi}(t+\phi\Delta t) \approx \phi\boldsymbol{\Psi}(\boldsymbol{u}(t+\Delta t))+(1-\phi)\boldsymbol{\Psi}(\boldsymbol{u}(t))$.

The differences are quite small between either formulation (both exhibiting similar orders of error) and we choose the latter. Therefore,

$$\begin{aligned}\boldsymbol{u}(t+\Delta t) = \boldsymbol{u}(t)+\boldsymbol{v}(t)\Delta t+\phi(\Delta t)^2\left(\phi\boldsymbol{\Psi}(t+\Delta t)\right. \\ \left.+(1-\phi)\boldsymbol{\Psi}(t)\right).\end{aligned} \tag{3.22}$$

When $\phi = 1$, then this approach can be considered to be a (implicit) Backward Euler scheme, which is very stable (very dissipative) and $\mathcal{O}((\Delta t)^2)$ locally in time, while if $\phi = 0$, the scheme can be considered as a (explicit) Forward Euler

scheme, which is conditionally stable and $\mathcal{O}((\Delta t)^2)$ locally in time and if $\phi = 0.5$, then the scheme can be considered as a (implicit) Midpoint scheme, which is marginally stable and $\hat{\mathcal{O}}((\Delta t)^2) = \mathcal{O}((\Delta t)^3)$ locally in time. The dependent plastic and damage variables are also integrated in a similar manner

$$\boldsymbol{\epsilon}(t+\Delta t) = \boldsymbol{\epsilon}(t) + \Delta t\,(\phi\dot{\boldsymbol{\epsilon}}(t+\Delta t) + (1-\phi)\dot{\boldsymbol{\epsilon}}(t)) \quad (3.23)$$

and

$$\mathcal{D}(t+\Delta t) = \mathcal{D}(t) + \Delta t\left(\phi\dot{\mathcal{D}}(t+\Delta t) + (1-\phi)\dot{\mathcal{D}}(t)\right). \quad (3.24)$$

3.2.2 Thermal fields

For the thermal field we write

$$\frac{\partial\theta}{\partial t} = \frac{1}{\rho C}\Big(\boldsymbol{\sigma} : (\dot{\boldsymbol{\epsilon}}_\theta + \dot{\boldsymbol{\epsilon}}_p) - \frac{1}{2}(\boldsymbol{\epsilon} - \boldsymbol{\epsilon}_\theta - \boldsymbol{\epsilon}_p) : \mathbb{E} : (\boldsymbol{\epsilon} - \boldsymbol{\epsilon}_\theta - \boldsymbol{\epsilon}_p) + \nabla_x \cdot (\mathbb{K} \cdot \nabla_x\theta) + \rho z\Big) \stackrel{\text{def}}{=} \boldsymbol{Y}. \quad (3.25)$$

We discretize for around the time $= t + \phi\Delta t$, yielding

$$\theta(t+\Delta t) \approx \theta(t) + \Delta t\,(\phi\boldsymbol{Y}(t+\Delta t) + (1-\phi)\boldsymbol{Y}(t))\,, \quad (3.26)$$

where the previously introduced spatial discretization is applied to the terms in $\boldsymbol{Y}$.

4 The overall solution scheme

In order to construct a solution, the algorithm is as follows:

(1) *Spatio-temporal discretization* Construct derivative terms such as

$$\frac{\partial u(x)}{\partial x} \approx \frac{u(x+\Delta x) - u(x-\Delta x)}{2\Delta x},\ etc \quad (4.1)$$

and insert into the governing equations. This leads to a system of coupled equations, for each node [(i, j, k) in Fig. 3], which are cast in the following (implicit/recursive) form [which are a recasting of the abstract system (Eqs. 3.1–3.2)]

$$\boldsymbol{u}(t+\Delta t) = \mathcal{F}(\boldsymbol{u}(t+\Delta t), \theta(t+\Delta t), \ldots), \quad (4.2)$$

and

$$\theta(t+\Delta t) = \mathcal{Y}(\boldsymbol{u}(t+\Delta t), \theta(t+\Delta t), \ldots). \quad (4.3)$$

(2) *System staggering* Compute $\boldsymbol{u}$-field with θ-fields fixed, then compute θ-field with $\boldsymbol{u}$-fields fixed, etc, and iterate at time interval $L+1$, $K = 1, 2\ldots$ for

$$\boldsymbol{u}^{L+1,K} = \mathcal{F}\left(\underline{\boldsymbol{u}^{L+1,K-1}}, \theta^{L+1.K-1}\right), \quad (4.4)$$

and

$$\theta^{L+1,K} = \mathcal{Y}\left(\boldsymbol{u}^{L+1,K}, \underline{\theta^{L+1.K-1}}\right), \quad (4.5)$$

Solving each of the above Eqs. (4.4 and 4.5), with the respective other fields fixed, can be achieved in a variety of ways, for example iteratively or by direct (Gaussian-type) solution methods (Fig. 3). For example, an interior iterative loop, within the staggering loop (within a time-step), can be used to update the solution to solve the individual field, for example the mechanical field, before moving to the next field (for example the thermal field). Those internal iterations can be performed until that individual field converges. This can then be repeated for the next field. This would

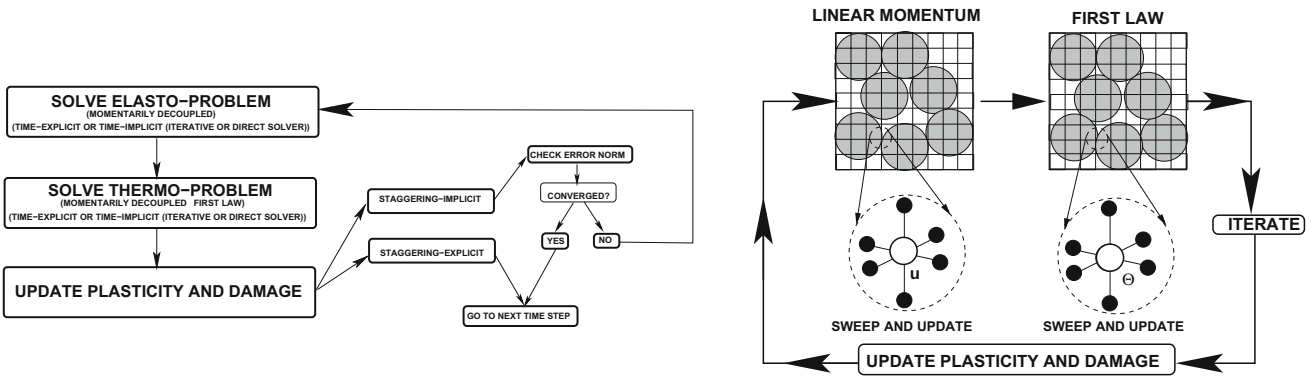

Fig. 3 The overall coupled staggering (*left*) solution and the matrix-free approach (*right*)

then complete one staggering iteration. There are of course many possible variants of this process. In theory, one could even simply perform an explicit update (no recursion). This is discussed further in the remarks that follow.

(3) Compute error measures: $\varpi^{*,K} \stackrel{\text{def}}{=} max(\varpi_u^K, \varpi_\theta^K)$, $i = 1, \ldots, nodes$ in the system.

(4a) If tolerance is met, $\varpi^{*,K} \leq C_{tol}$ and $K \leq K_d$, then:

(i) Increment time forward: $t = t + \Delta t$,

(ii) Construct new time step: $(\Delta t)^{\text{new}} = \Phi_K (\Delta t)^{\text{old}}$, where $\Phi_K \stackrel{\text{def}}{=} \left(\frac{\left(\frac{C_{tol}}{\varpi^{*,0}}\right)^{\frac{1}{pK_d}}}{\left(\frac{\varpi^{*,K}}{\varpi^{*,0}}\right)^{\frac{1}{pK}}} \right)$

(iii) Select $\Delta t = min((\Delta t)^{lim}, \Delta t)$ and go to (1)

(4b) If tolerance is not met, $\varpi^{*,K} > C_{tol}$ and $K = K_d$, then construct (refine) new time step: $(\Delta t)^{\text{new}} \stackrel{\text{def}}{=} \Phi_K (\Delta t)^{\text{old}}$

$$\Phi_K \stackrel{\text{def}}{=} \left(\frac{\left(\frac{C_{tol}}{\varpi^{*,0}}\right)^{\frac{1}{pK_d}}}{\left(\frac{\varpi^{*,K}}{\varpi^{*,0}}\right)^{\frac{1}{pK}}} \right) \tag{4.6}$$

and go to (1). This time-scaling relation is derived in Appendix 1.

At a given time, once the process is complete, then the time is incremented forward and the process is repeated. The overall goal is to deliver solutions where the iterative error is controlled and the temporal discretization accuracy dictates the upper limit on the time step size (Δt^{lim}). Clearly, there are various combinations of solution methods that one can choose from. For example, for the overall field coupling, one may choose implicit or explicit staggering and within the staggering process, either implicit ($0 < \phi \leq 1$) or explicit time-stepping ($\phi = 0$), and, as mentioned previously in the case of implicit time-stepping, iterative or direct solvers for the balance of linear momentum and the first law of thermodynamics (Fig. 3).

4.1 Algorithmic observation 1

It is important to emphasize that one should use the previous (converged) time step's solution as the starting guess for the next time step to obtain a "head-start" $\left(\boldsymbol{u}^{K=0}(t + \Delta t) = \boldsymbol{u}(t)\right)$. When selecting a time step, one must balance accuracy concerns and, simultaneously, stability issues.[4] Clearly, the smaller the time-step, the more stable the solution process, however, more time steps implies more system evaluations. Since the multifield staggering scheme iterates anyway, implicit methods are preferred for the applications of interest. As the physics changes, the field that is most sensitive (exhibits the largest amount of relative nondimensional change) dictates the time-step size. Because the internal system solvers within the staggering scheme are also iterative and use the previously converged solution as their starting value to solve the system of equations, a field that is relatively insensitive at given stage of the simulation will converge in a very few internal iterations (perhaps even one).

[4] Typically, the number of iterations needed to solve the coupled system, if an iterative scheme is used, increases with the time step size and the value of ϕ.

4.2 Algorithmic observation 2

Generally speaking, the solution to the individual field equations progresses in a node by node fashion whereby, at a node (i, j, k), for example for the mechanical field calculations, one has in an abstract form

$$\boldsymbol{u}(t + \Delta t) \approx \mathcal{F}(\boldsymbol{u}(t), \boldsymbol{u}(t + \Delta t), \theta(t), \theta(t + \Delta t)), \tag{4.7}$$

where the term on the lefthand side is updated and the terms on the right are previous iterate (old) values. This entails using the old values for all finite difference stencils that eventually become updated only after the algorithm completely traverse through the system, updating values, node by node (*no matrices need to be formed*, Fig. 3). There exist many methods to accelerate such computations, such as Successive Over-Relaxation, based on the pioneering work of Young [76]. For reviews, see Ames [3] or Axelsson [5]. Note that for the mechanical field calculations the thermal field is instantaneously fixed, and are updated only when it is to be solved, in the staggered manner (fixing the mechanical variables). At the algebraic equation solution level, after the individual field has been solved, the entire solution is passed to the next field equation, as described in the previous algorithm (Fig. 3). This is a Jacobi-type scheme, whereby the updates are made only after one complete system iteration, which is easier to address theoretically, as opposed to a Gauss-Seidel type method, which involves immediately using the most current field values, when they become available. The Jacobi method is easily parallelizable, if desired. In other words, the calculation for each node is (momentarily) uncoupled, with the updates only coming at the end of an iteration. Gauss-Seidel, since it requires the most current updates, couples the nodal calculations immediately.

5 Numerical examples

As a model problem, we consider a group of particles with a smaller scale interstitial (compacted very fine particle) material that is assumed to be a continuous phase. We generated

a group of N_p randomly dispersed spherical particles, of equal size, embedded in a cubical domain of dimensions, $D \times D \times D$. The particle size was determined by a particle/sample size ratio, which was defined via a subvolume size $V \overset{\text{def}}{=} \frac{D \times D \times D}{N_p}$. The non-dimensional ratio between the particle radii (b) and the subvolume was denoted by $\mathcal{L} \overset{\text{def}}{=} \frac{b}{V^{\frac{1}{3}}}$. The volume fraction occupied by the particles consequently can be written as $v_p \overset{\text{def}}{=} \frac{4\pi \mathcal{L}^3}{3}$. Thus, the total volume occupied by the particles denoted ζ, can be written as $\zeta = v_p N_p V$. Large values of $\zeta > 0.5$ allow for overlap. We used $N_p = 100$ particles (Fig. 4). This sample size was arrived at by successively enlarging sample until there were no significant changes in the overall system response for further enlargements. The classical random sequential addition algorithm was used to place nonoverlapping particles randomly into the domain of interest (RSA; Widom [75]). The particles were then enlarged from those locations and allowed to overlap.

Remark For higher volumes fraction during the first phase of this algorithm (particle placement), more sophisticated algorithms, such as the equilibrium-based, Metropolis algorithm can be used or methods based on simultaneous particle flow and growth, found in Torquato [72], Kansaal et al. [39] and Donev et al. [15–19].

5.1 Sample size selection

In order to select a suitable sample that is statistically representative (a RVE), we employ a "framing" method, whereby the boundary conditions are applied ($\boldsymbol{u}$ and θ) to the boundary of a sample (Fig. 4), and an interior subsample is used to probe what the material would experience without the direct influence of the applied boundary conditions. This approach avoids introducing boundary layer effects into the interior response. For more details, see Zohdi [85,87]. An implementation of a "framing" approach is as follows:

- *STEP (1)* Generate a sample with a certain number of particles in its interior,
- *STEP (2)* For the effective property calculation (averaging), select a subsample ("a sub-box", Fig. 4) in the interior (to avoid boundary layer effects that arise from the imposition of boundary conditions),
- *STEP (3)* Repeat STEPS (1) and (2) for different random realizations for a given sample size, and average the resulting response to determine a mean value,
- *STEP (4)* Repeat STEPS (1)–(3) for a larger sample,
- *STEP (5)* Continue the process (STEPS (1)–(4)) until the response ceases to change to within an acceptable tolerance.

For a more in depth discussion on size-effect issues, see the works of Zohdi [79,81,84,85] and [87].

5.2 Numerical examples

As an example, the following parameters were used:

- reference temperature, $\theta_r = 600\,^{\circ}\text{K}$,
- initial temperature, $\theta_0 = 600\,^{\circ}\text{K}$,
- total time, $T = 10^{-5}$ s,
- initial time step size, $\Delta t = 10^{-10}$ s,
- damage lower bound, $\alpha = 0.1$,
- displacement loading on all sides $\boldsymbol{u} = (0, 0, 0)$ m,

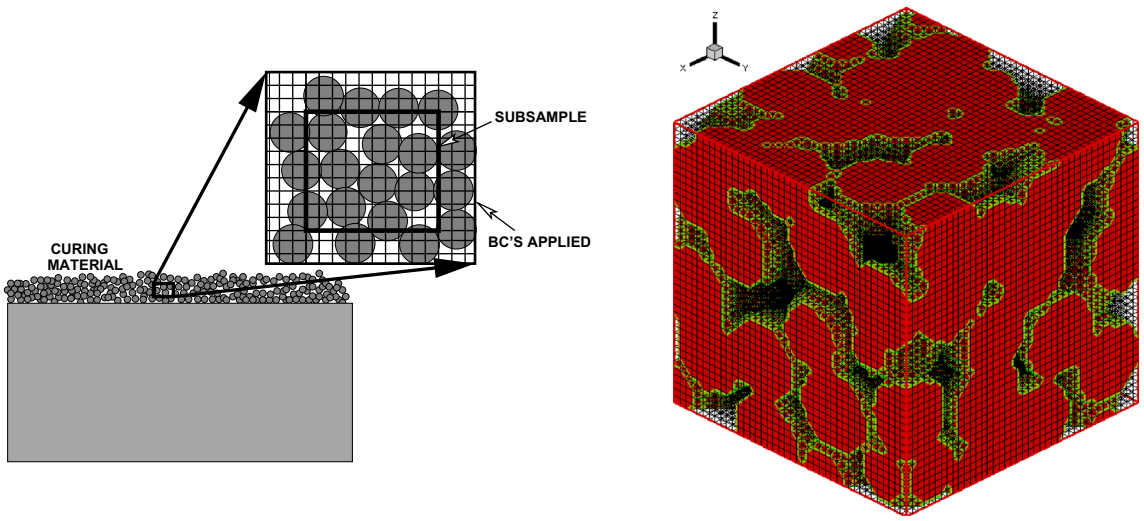

Fig. 4 *LEFT* Hot deposited particles on a surface. With the framing method, a sample is probed with interior subsamples, within the larger sample, in order to avoid boundary layer effects that occur from imposing boundary conditions on the large-sample exterior. *RIGHT* A mesh of the curing subsample (showing only one of the particle phases for illustration purposes)

- temperature of all sides, $\theta(t) = -300^\circ \frac{t}{T} + 600\,^\circ\text{K}$,
- dimensions of the sample, $0.001 \times 0.001 \times 0.001$ m,
- particles in the sample, $N_p = 100$,
- base density, $\rho = 1000\,\text{kg/m}^3$,
- base Lame parameters, $\lambda_o = 10$ GPa, $\mu_o = 3$ GPa,
- base conductivity, $\boldsymbol{I\!K}_o = K_o \mathbf{1}$, $K_o = 100$ W/K° m,
- base thermal expansion coefficient, $\beta_o = 0.000001$ 1/°K,
- base heat capacity, $C_o = 10$ J/K° kg,
- base plastic rate coefficient, $a_o = 0.001$,
- base yield stress, $\sigma_{yo} = 10$ MPa,
- base damage rate coefficient, $b_o = -10000000$,
- base damage flow stress, $\sigma_{do} = 10$ MPa,
- relative densities, $\rho_{1r} = \frac{\rho_1}{\rho} = 1$, $\rho_{2r} = \frac{\rho_2}{\rho} = 2$,
- relative Lame parameters, $\lambda_{1r} = \frac{\lambda_1}{\lambda_o}$, $\lambda_{2r} = \frac{\lambda_2}{\lambda_o} = 5$,
- relative Lame parameters, $\mu_{1r} = \frac{\mu_1}{\mu_o} = 1$, $\mu_{2r} = \frac{\mu_2}{\mu_o} = 5$,
- relative conductivity, $K_{1r} = \frac{\boldsymbol{I\!K}_1}{\boldsymbol{I\!K}_o} = 1$, $K_{2r} = \frac{\boldsymbol{I\!K}_2}{\boldsymbol{I\!K}_o} = 5$,
- relative thermal expansion, $\beta_{1r} = \frac{\beta_1}{\beta_o} = 1$, $\beta_{2r} = \frac{\beta_2}{\beta_o} = 10$,
- relative heat capacity, $C_{1r} = \frac{C_1}{C_o} = 1$, $C_{2r} = \frac{C_2}{C_o} = 2$,
- relative plastic rate coefficient, $a_{1r} = \frac{a_1}{a_o} = 1$, $a_{2r} = \frac{a_2}{a_o} = 1$,
- relative damage rate coefficient, $b_{1r} = \frac{b_1}{b_o} = 1$, $b_{2r} = \frac{b_2}{b_o} = 1$,
- relative plastic yield, $\sigma_{y1r} = \frac{\sigma_{y1}}{\sigma_{yo}} = 1$, $\sigma_{y2r} = \frac{\sigma_{y2}}{\sigma_{yo}} = 5$,
- relative damage threshold, $\sigma_{d1r} = \frac{\sigma_{d1}}{\sigma_{do}} = 1$, $\sigma_{d1r} = \frac{\sigma_{d2}}{\sigma_{do}} = 5$,
- a time stepping factor $\phi = 0.5$ (mid-point rule),
- an overlapping length scale of the particles of $\zeta = 0.625$,
- the number of desired iterations per time step set to $K_d = 5$, along with a coupling/staggering tolerance of $C_{tol} = 10^{-2}$,
- weights for the iterative error norm, $w_1 = 0.5$ and $w_2 = 0.5$.

Throughout the computations, the spatial discretization meshes were repeatedly refined until the solutions did not exhibit any more sensitivity to further refinement of the grid-spacing. We started with meshes such as a $21 \times 21 \times 21$ mesh, arising from having a cubical mesh with 10 nodes from the centerline plane of symmetry and one node in the middle, and then repeatedly refined in the following sequential manner:

1. *Mesh* # 1 a $21 \times 21 \times 21$ mesh, which has 9261 degrees of freedom (DOF) for the thermal field and 27,783 DOF for the mechanical field, for a total of 37,044 DOF.
2. *Mesh* # 2 a $41 \times 41 \times 41$ mesh, which has 68921 degrees of freedom (DOF) for the thermal field and 206783 DOF for the mechanical field, for a total of 275,684 DOF.
3. *Mesh* # 3 a $61 \times 61 \times 61$ mesh, which has 226,981 degrees of freedom (DOF) for the thermal field and 680,943 DOF for the mechanical field, for a total of 907,924 DOF.
4. *Mesh* # 4 a $81 \times 81 \times 81$ mesh, which has 531,441 degrees of freedom (DOF) for the thermal field and 1,594,322 DOF for the mechanical field, for a total of 2,125,764 DOF.

Approximately between a 61-level and a 81-level mesh, the results stabilized, indicating that the results are essentially free of any appreciable numerical error. *All numerical results are shown in* Figs. 5, 6, 7, 8. At the length-scales of interest, it is questionable whether the ideas of a sharp material interface are justified. Accordingly, we simulated the system with and without Laplacian smoothing, whereby one smooths the material data by post-processing the material data, node by node, to produce a smoother material representation, for example, for the thermal conductivity, $\hat{\boldsymbol{I\!K}}$ (using the stencil in Fig. 9 in the Appendix 1)

$$\nabla_x^2 \boldsymbol{I\!K} = \mathbf{0} \Rightarrow \hat{\boldsymbol{I\!K}}_{i,j,k} = \frac{1}{6}\left(\boldsymbol{I\!K}_{i+1,j,k} + \boldsymbol{I\!K}_{i-1,j,k} + \boldsymbol{I\!K}_{i,j+1,k} + \boldsymbol{I\!K}_{i,j-1,k} + \boldsymbol{I\!K}_{i,j,k+1} + \boldsymbol{I\!K}_{i,j,k-1}\right). \tag{5.1}$$

The same was done for the mechanical properties by enforcing $\nabla_x^2 \lambda_0 = \mathbf{0}$ and $\nabla_x^2 \mu_0 = \mathbf{0}$ and as well as other material data. The simulations were run with and without data smoothing, with the results being negligibly different for sufficiently fine meshes (Fig. 4). In particular, Fig. 4 depicts a typical microstructure showing the contact area (only illustrating one of the phases), while Fig. 5 shows successive frames of the deviatoric stress, 25 % into the interior of the sample. Figures 6, 7, 8 illustrate the various metrics that a materials designer would be interested in quantifying. In Fig. 8, the variation of the time step size (normalized by the starting time step size) is depicted. The size of the time steps were purposely started quite small ($\Delta t = 10^{-10}$ s) and given an enlargement cap of 50 times in magnitude. This allows the system to slowly evolve to capture the quite transient behavior. During the bulk of the computation, the large steps were warranted (the time-step size evolved), as dictated by the physics and the adaptive algorithm. For other material selections and loading regimes, other adaptivity modes can occur. All simulations were run on a standard laptop requiring minimal memory requirements. It is important to stress that it is virtually impossible to determine a-priori whether the initial time step is adequate to meet a tolerance and whether adaptivity is needed. *Obviously, we can use this scheme for any (trapezoidal) value of* $0 \leq \phi \leq 1$. Time-step size adaptivity is important, since the solution can drastically change over the course of time, possibly requiring quite different time step sizes to control the iterative (staggering) error. However, to

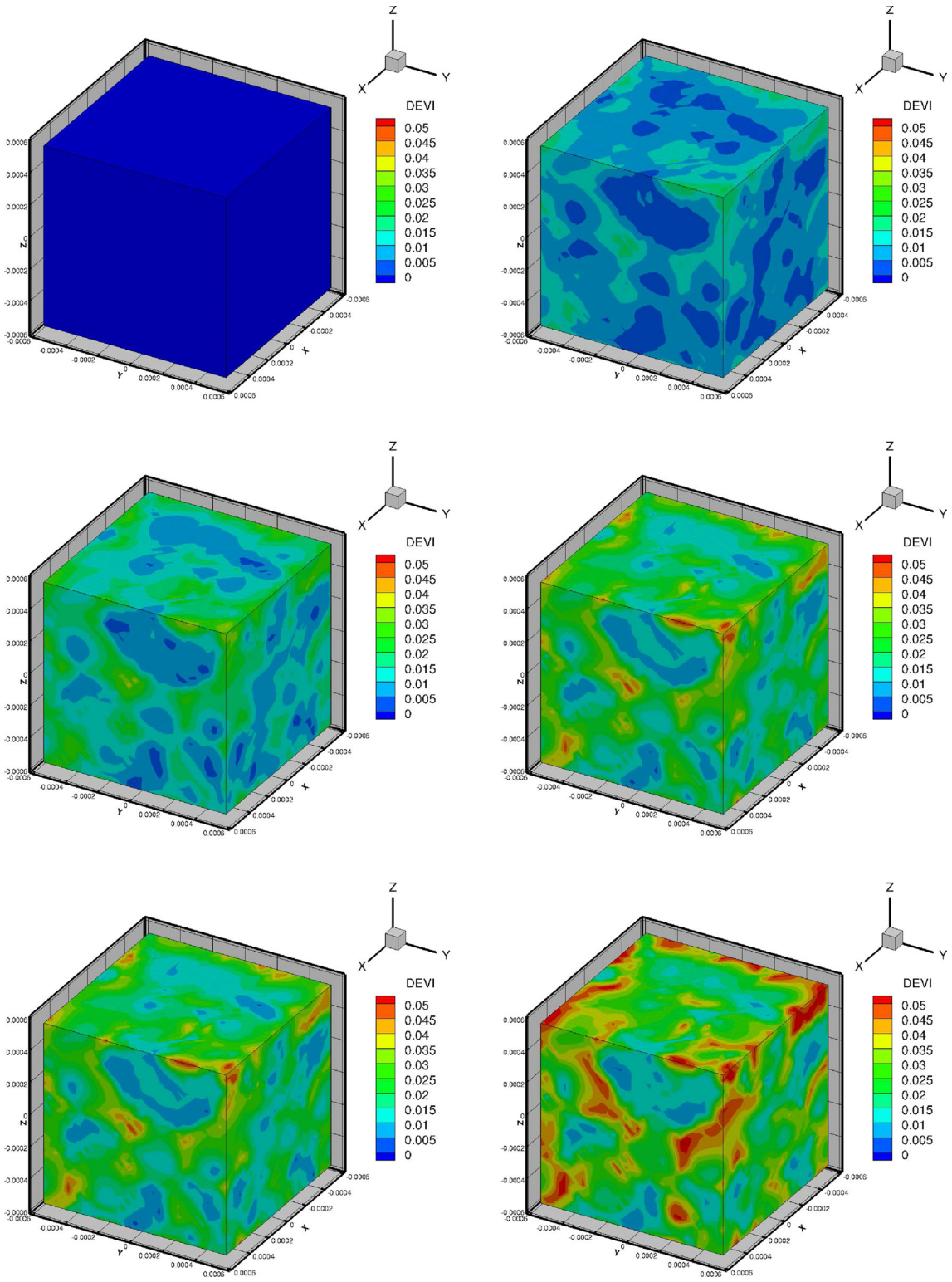

Fig. 5 From left to right and top to bottom: the evolution of the deviatoric stress (in gigapascals). Starting from the top left, a uniform low stress exists in the hot mixture. Thereafter because of the heterogeneous nature of the material properties, large differences arise in the stress state as the material cools. Note: The morphology is shown in Fig. 4

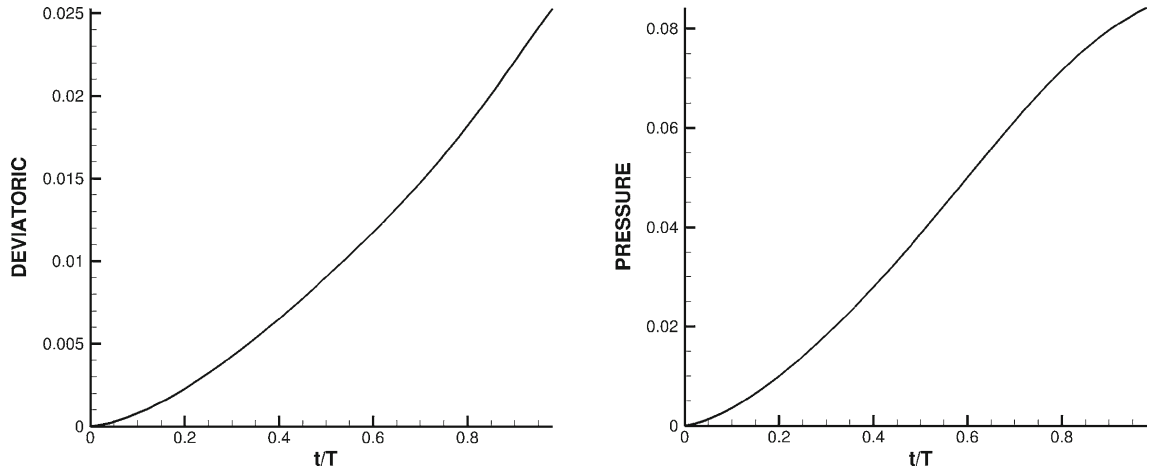

Fig. 6 *LEFT* The volume averaged normed deviator $||\boldsymbol{\sigma}'||$ (in gigapascals). *RIGHT* The volume averaged pressure $p \stackrel{\text{def}}{=} \frac{tr\boldsymbol{\sigma}}{3}$ (in gigapascals)

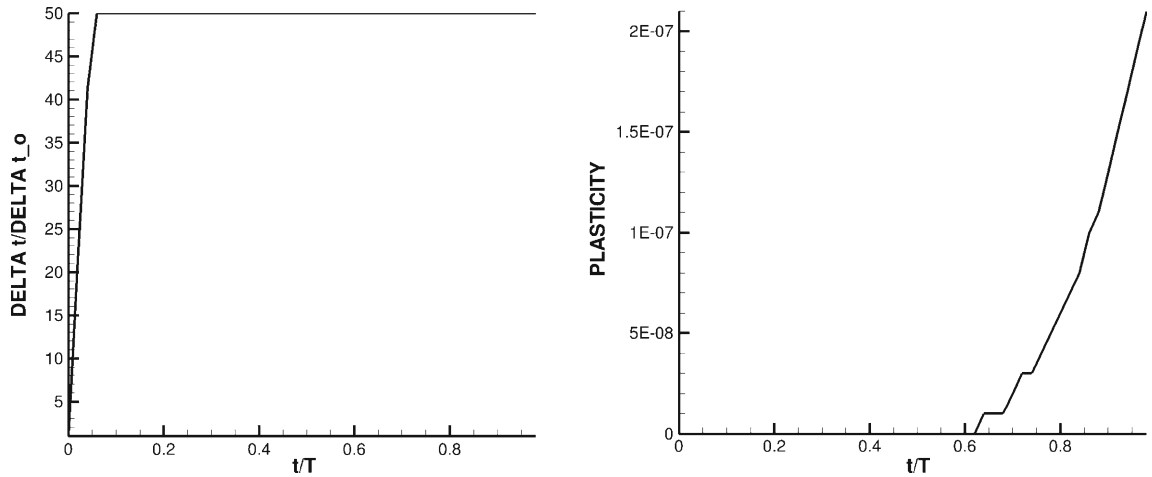

Fig. 7 *LEFT* The volume averaged temperature $\langle\theta\rangle_\Omega$ (in Kelvin) *RIGHT* The volume averaged norm of the plastic strain $||\boldsymbol{\epsilon}_p||$

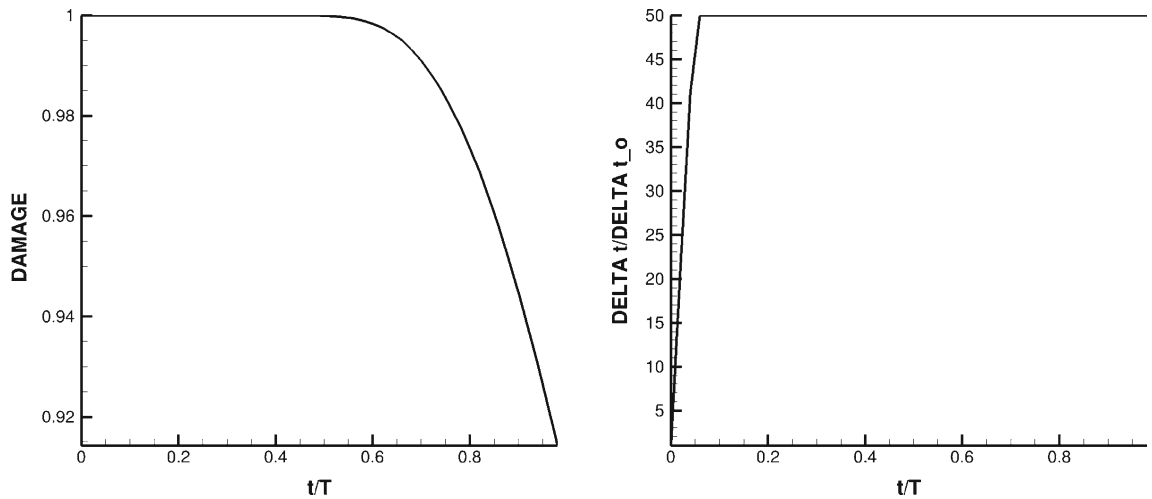

Fig. 8 *LEFT* The volume averaged damage $||\mathcal{D}||$. *RIGHT* The time-step size variation

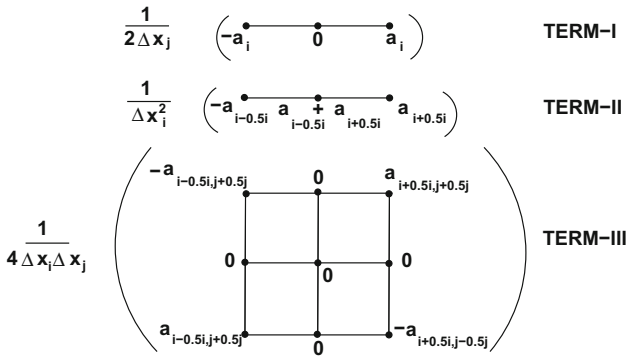

Fig. 9 Various Finite-difference stencils in "computational molecule" form (centered at (x_i, x_j, x_k)), where: (*1*) TERM-I: $a\frac{\partial u}{\partial x_i}$, (*2*) TERM-II: $\frac{\partial}{\partial x_i}\left(a\frac{\partial u}{\partial x_i}\right)$ and (*3*) TERM-III: $\frac{\partial}{\partial x_j}\left(a\frac{\partial u}{\partial x_i}\right)$

maintain the accuracy of the time-stepping scheme, one must respect an upper bound dictated by the discretization error, i.e., $\Delta t \leq \Delta t^{lim}$. The example shown was simply to illustrate the overall process.

Remark While our stated focus is the evolution of stresses in deposited hot powders/particles a by-product of the analysis overall effective mechanical stiffness relation defined by

$$\langle \boldsymbol{\sigma} \rangle_\Omega = \mathcal{F}^*(\langle \boldsymbol{\epsilon} \rangle_\Omega), \tag{5.2}$$

where $\langle \cdot \rangle_\Omega \overset{\text{def}}{=} \frac{1}{|\Omega|}\int_\Omega \cdot \, d\Omega$. Similarly, one can generate effective thermal responses

$$\langle \boldsymbol{q} \rangle_\Omega = \mathcal{G}^*(\langle \nabla\theta \rangle_\Omega). \tag{5.3}$$

There are a variety of estimates for effective responses in many fields. We refer the reader to Hashin and Shtrikman [30] based on variational principles using the concept of polarization tensor fields (filtering/separation of micro-macro scales) and numerical techniques to extract the effective response of such materials (Zohdi [84]). Estimates for the effective properties of heterogeneous materials date back over 150 years to Maxwell [49] and [50] and Lord Rayleigh [61]. For a relatively recent and thorough analysis of a variety of classical approaches, such as the ones briefly mentioned here, see Torquato [72] for general interdisciplinary discussions, Jikov et al. [34] for more mathematical aspects, Hashin [31], Mura [51], Nemat-Nasser and Hori [55] for solid-mechanics inclined accounts of the subject, for analyses of defect-laden, porous and cracked media, see Kachanov [36], Kachanov, Tsukrov and Shafiro [37], Kachanov and Sevostianov [38], Sevostianov, Gorbatikh and Kachanov [66], Sevostianov and Kachanov [67], and for computational aspects see Ghosh [26], Ghosh and Dimiduk [27], Zohdi and Wriggers [84] and Zohdi [87].

6 Summary and extensions

6.1 Summary

The overall goal of this research was to develop a computational framework that is relatively easy to implement in order to analyze deposited hot particulate microstructures undergoing cooling. Specifically, a computational approach that efficiently resolves the strongly coupled time-transient thermo-mechanical stress fields that arise, built on a direct discretization of a deposited microstructure and an iterative staggering scheme, was developed. The spatial discretization grids used were uniform and dense, and the deposited microstructure was embedded into spatial discretization. The regular grid allows one to generate a matrix-free iterative formulation which is amenable to rapid calculation and minimal memory requirements, making it ideal for laptop computation. Variants of the technique have been applied to related problems involving more coupled multiphysics, such as electro-magneto-thermo-mechano-chemo effects, in Zohdi [85] whereby one computes the electrical $\boldsymbol{E}$-field with the magnetic field $\boldsymbol{H}$, thermal field θ, displacement field $\boldsymbol{u}$ and chemical field c fixed, then computes $\boldsymbol{H}$-field with $\boldsymbol{E}$, θ, $\boldsymbol{u}$ and c fields fixed, etc, and iterates at time interval $L+1$, $K = 1, 2 \ldots$ for (written directly in iterative implicit form)

$$\boldsymbol{E}^{L+1,K} = \mathcal{F}\left(\underline{\boldsymbol{E}^{L+1,K-1}}, \boldsymbol{H}^{L+1,K-1}, \theta^{L+1.K-1}, \boldsymbol{u}^{L+1.K-1}, c^{L+1.K-1}\right), \tag{6.1}$$

and

$$\boldsymbol{H}^{L+1,K} = \mathcal{G}\left(\boldsymbol{E}^{L+1,K}, \underline{\boldsymbol{H}^{L+1,K-1}}, \theta^{L+1.K-1}, \boldsymbol{u}^{L+1.K-1}, c^{L+1.K-1}\right), \tag{6.2}$$

and

$$\theta^{L+1,K} = \mathcal{Y}\left(\boldsymbol{E}^{L+1,K}, \boldsymbol{H}^{L+1,K}, \underline{\theta^{L+1.K-1}}, \boldsymbol{u}^{L+1.K-1}, c^{L+1.K-1}\right), \tag{6.3}$$

and

$$\boldsymbol{u}^{L+1,K} = \mathcal{L}\left(\boldsymbol{E}^{L+1,K}, \boldsymbol{H}^{L+1,K}, \theta^{L+1.K}, \underline{\boldsymbol{u}^{L+1.K-1}}, c^{L+1.K-1}\right), \tag{6.4}$$

and

$$c^{L+1,K} = \mathcal{C}\left(\boldsymbol{E}^{L+1,K}, \boldsymbol{H}^{L+1,K}, \theta^{L+1.K}, \boldsymbol{u}^{L+1.K}, \underline{c^{L+1.K-1}}\right), \tag{6.5}$$

where the only underlined variable is active at that stage of the process. One then computes the maximum of the error measures $\varpi^{*,K} \stackrel{\text{def}}{=} max\left(\varpi_E^K, \varpi_H^K, \varpi_\theta^K, \varpi_u^K, \varpi_c^K\right)$ in order to determine if time-step adaptivity is necessary, as introduced earlier for the thermo-mechanical scheme. Generally, the methods discussed in this work can be combined to create hybrid block-partitioned approaches, whereby the entire domain is partitioned into subdomains and within each subdomain an iterative method is applied. In other words, for a subdomain, the values at all nodes from outside are initially frozen, as far as calculations involving members of the group are concerned. After each isolated subdomain's solution (nodal values) has converged (computed in parallel), then all nodal values are updated, i.e. the most current values become available to all members of the grid, and the isolated subdomain calculations are repeated. Although parallel computation of the introduced algorithms was not pursued in this work, it is currently being investigated by the author. Finally, we remark that often the use of lasers is a critical component of the types of processes described in this paper, specifically to selectively control the temperature in targeted zones (Zohdi [92]). In particular, for deposited particle-based materials, selective thermal processing using lasers (or variants based on electron beams) is quite attractive. The upper bound for the power of a typical industrial laser is approximately 10,000 W. Typically, the initial beam produced is in the form of collimated (parallel) beams which are then focused with a lens onto a small focal point (approximately 50 mm away) of no more than about 0.000025 m in diameter. Selective laser processing/sintering, was pioneered by Householder [32] in 1979 and Deckard and Beamen [13] in the mid-1980s.[5] Generally, an overall future computational technological goal is to develop simulation tools to accelerate the manufacturing of printed electronics. *Lasers can play a central role in precisely processing these systems.* To describe the *laser-target* interaction, the following must be accounted for: (a) absorption of laser energy input, (b) beam interference (attenuation) from the heterogeneous media and (c) heat transfer by conduction. Integration of laser input into the models described in this paper is currently being pursued by the author based on Zohdi [83,89,92].

Appendix 1: Spatial finite difference stencils

The following standard approximations are used:

1. For the first derivative of a primal variable u at (x_1, x_2, x_3):

$$\frac{\partial u}{\partial x_1} \approx \frac{u(x_1 + \Delta x_1, x_2, x_3) - u(x_1 - \Delta x_1, x_2, x_3)}{2\Delta x_1} \tag{7.1}$$

2. For the derivative of a flux at (x_1, x_2, x_3), with an arbitrary material coefficient a:

$$\begin{aligned}
&\frac{\partial}{\partial x_1}\left(a\frac{\partial u}{\partial x_1}\right) \\
&\approx \frac{\left(a\frac{\partial u}{\partial x_1}\right)|_{x_1+\frac{\Delta x_1}{2},x_2,x_3} - \left(a\frac{\partial u}{\partial x_1}\right)|_{x_1-\frac{\Delta x_1}{2},x_2,x_3}}{\Delta x_1} \\
&= \frac{1}{\Delta x_1}\left[a(x_1 + \frac{\Delta x_1}{2}, x_2, x_3)\right. \\
&\quad \left.\times\left(\frac{u(x_1 + \Delta x_1, x_2, x_3) - u(x_1, x_2, x_3)}{\Delta x_1}\right)\right] \\
&\quad - \frac{1}{\Delta x_1}\left[a(x_1 - \frac{\Delta x_1}{2}, x_2, x_3)\right. \\
&\quad \left.\times\left(\frac{u(x_1, x_2, x_3) - u(x_1 - \Delta x_1, x_2, x_3)}{\Delta x_1}\right)\right],
\end{aligned} \tag{7.2}$$

where we have used

$$\begin{aligned}
a(x_1 + \frac{\Delta x_1}{2}, x_2, x_3) \approx \frac{1}{2}\,&(a(x_1 + \Delta x_1, x_2, x_3) \\
&+ a(x_1, x_2, x_3))
\end{aligned} \tag{7.3}$$

and

$$\begin{aligned}
a(x_1 - \frac{\Delta x_1}{2}, x_2, x_3) \approx \frac{1}{2}\,&(a(x_1, x_2, x_3) \\
&+ a(x_1 - \Delta x_1, x_2, x_3))
\end{aligned} \tag{7.4}$$

3. For the cross-derivative of a flux at (x_1, x_2):

$$\begin{aligned}
&\frac{\partial}{\partial x_2}\left(a\frac{\partial u}{\partial x_1}\right) \approx \frac{\partial}{\partial x_2}\,(a(x_1, x_2, x_3) \\
&\quad \times\left(\frac{u(x_1 + \Delta x_1, x_2, x_3) - u(x_1 - \Delta x_1, x_2, x_3)}{2\Delta x_1}\right)\Big) \\
&\approx \frac{1}{4\Delta x_1 \Delta x_2}(a(x_1, x_2 + \Delta x_2, x_3)\,[u(x_1 + \Delta x_1, x_2 \\
&\quad + \Delta x_2, x_3) - u(x_1 - \Delta x_1, x_2 + \Delta x_2, x_3)] \\
&\quad - a(x_1, x_2 - \Delta x_2, x_3)\,[u(x_1 + \Delta x_1, x_2 - \Delta x_2, x_3) \\
&\quad - u(x_1 - \Delta x_1, x_2 - \Delta x_2, x_3)]),
\end{aligned} \tag{7.5}$$

[5] A closely related method, Electron Beam Melting, fully melts the material and produces dense solids that are void free.

Remark To illustrate second-order accuracy, consider a Taylor series expansion for an arbitrary function u

$$u(x+\Delta x) = u(x) + \frac{\partial u}{\partial x}\bigg|_x \Delta x + \frac{1}{2}\frac{\partial^2 u}{\partial x^2}\bigg|_x (\Delta x)^2 + \frac{1}{6}\frac{\partial^3 u}{\partial x^3}\bigg|_x (\Delta x)^3 + \mathcal{O}\left((\Delta x)^4\right) \tag{7.6}$$

and

$$u(x-\Delta x) = u(x) - \frac{\partial u}{\partial x}\bigg|_x \Delta x + \frac{1}{2}\frac{\partial^2 u}{\partial x^2}\bigg|_x (\Delta x)^2 - \frac{1}{6}\frac{\partial^3 u}{\partial x^3}\bigg|_x (\Delta x)^3 + \mathcal{O}\left((\Delta x)^4\right) \tag{7.7}$$

Subtracting the two expressions yields

$$\frac{\partial u}{\partial x}|_x = \frac{u(x+\Delta x) - u(x-\Delta x)}{2\Delta x} + \mathcal{O}\left((\Delta x)^2\right). \tag{7.8}$$

Appendix 2: temporally-adaptive iterative methods

Implicit time-stepping methods, with time step size adaptivity, built on approaches found in Zohdi [79,82,85,88] and [90] were used throughout the analysis in the body of the work. In order to introduce basic concepts, we consider a first order differential equation for a field $\boldsymbol{W}$:

$$\dot{\boldsymbol{W}} = \boldsymbol{\Lambda}(\boldsymbol{W}), \tag{8.1}$$

which, after being discretized using a trapezoidal "ϕ-method" ($0 \leq \phi \leq 1$)

$$\boldsymbol{W}^{L+1} = \boldsymbol{W}^{L} + \Delta t\left(\phi\boldsymbol{\Lambda}\left(\boldsymbol{W}^{L+1}\right) + (1-\phi)\boldsymbol{\Lambda}\left(\boldsymbol{W}^{L}\right)\right). \tag{8.2}$$

Generally, for systems of equations of this form, a straightforward iterative scheme can be written as

$$\boldsymbol{W}^{L+1,K} = \mathcal{G}\left(\boldsymbol{W}^{L+1,K-1}\right) + \mathcal{R}, \tag{8.3}$$

where $\mathcal{R}$ is a remainder term that does not depend on the solution, i.e. $\mathcal{R} \neq \mathcal{R}(\boldsymbol{W}^{L+1})$, and $K = 1, 2, 3, \ldots$ is the index of iteration within time step $L+1$. The convergence of such a scheme is dependent on the behavior of $\mathcal{G}$. Namely, a sufficient condition for convergence is that $\mathcal{G}$ is a contraction mapping for all $\boldsymbol{W}^{L+1,K}$, $K = 1, 2, 3 \ldots$ In order to investigate this further, we define the iteration error as

$$\varpi^{L+1,K} \stackrel{\text{def}}{=} ||\boldsymbol{W}^{L+1,K} - \boldsymbol{W}^{L+1}||. \tag{8.4}$$

A necessary restriction for convergence is iterative self consistency, i.e. the "exact" (discretized) solution must be represented by the scheme

$$\mathcal{G}\left(\boldsymbol{W}^{L+1}\right) + \mathcal{R} = \boldsymbol{W}^{L+1}. \tag{8.5}$$

Enforcing this restriction, a sufficient condition for convergence is the existence of a contraction mapping

$$\begin{aligned} \varpi^{L+1,K} &= ||\boldsymbol{W}^{L+1,K} - \boldsymbol{W}^{L+1}|| \\ &= ||\mathcal{G}(\boldsymbol{W}^{L+1,K-1}) - \mathcal{G}(\boldsymbol{W}^{L+1})|| \qquad (8.6) \\ &\leq \eta^{L+1,K}||\boldsymbol{W}^{L+1,K-1} - \boldsymbol{W}^{L+1}||, \qquad (8.7) \end{aligned}$$

where, if $0 \leq \eta^{L+1,K} < 1$ for each iteration K, then $\varpi^{L+1,K} \rightarrow 0$ for any arbitrary starting value $\boldsymbol{W}^{L+1,K=0}$, as $K \rightarrow \infty$. This type of contraction condition is sufficient, but not necessary, for convergence. Inserting these approximations into $\dot{\boldsymbol{W}} = \boldsymbol{\Lambda}(\boldsymbol{W})$ leads to

$$\boldsymbol{W}^{L+1,K} \approx \underbrace{\Delta t\left(\phi\boldsymbol{\Lambda}(\boldsymbol{W}^{L+1,K-1})\right)}_{\mathcal{G}(\boldsymbol{W}^{L+1,K-1})} + \underbrace{\Delta t(1-\phi)\boldsymbol{\Lambda}(\boldsymbol{W}^{L}) + \boldsymbol{W}^{L}}_{\mathcal{R}}, \tag{8.8}$$

whose contraction constant is scaled by $\eta \propto \phi\Delta t$. Therefore, if convergence is slow within a time step, the time step size, which is adjustable, can be reduced by an appropriate amount to increase the rate of convergence. Decreasing the time step size improves the convergence, however, we want to simultaneously maximize the time-step sizes to decrease overall computing time, while still meeting an error tolerance on the numerical solution's accuracy. In order to achieve this goal, we follow an approach found in Zohdi [79,82,85,88] and [90] originally developed for continuum thermo-chemical multi-field problems in which one first approximates

$$\eta^{L+1,K} \approx S(\Delta t)^p \tag{8.9}$$

(S is a constant) and secondly one assumes the error within an iteration to behave according to

$$(S(\Delta t)^p)^K \varpi^{L+1,0} = \varpi^{L+1,K}, \tag{8.10}$$

$K = 1, 2, \ldots$, where $\varpi^{L+1,0}$ is the initial norm of the iterative error and S is intrinsic to the system.[6] Our goal is to meet an error tolerance in exactly a preset number of iterations. To this end, one writes

$$(S(\Delta t_{\text{tol}})^p)^{K_d} \varpi^{L+1,0} = C_{tol}, \tag{8.11}$$

[6] For the class of problems under consideration, due to the linear dependency on Δt, $p \approx 1$.

where C_{tol} is a (coupling) tolerance and where K_d is the number of desired iterations.[7] If the error tolerance is not met in the desired number of iterations, the contraction constant $\eta^{L+1,K}$ is too large. Accordingly, one can solve for a new smaller step size, under the assumption that S is constant,

$$\Delta t_{\text{tol}} = \Delta t \left(\frac{\left(\frac{C_{tol}}{\varpi^{L+1,0}} \right)^{\frac{1}{pK_d}}}{\left(\frac{\varpi^{L+1,K}}{\varpi^{L+1,0}} \right)^{\frac{1}{pK}}} \right). \tag{8.12}$$

The assumption that S is constant is not critical, since the time steps are to be recursively refined and unrefined throughout the simulation. Clearly, the expression in Eq. 8.12 can also be used for time step enlargement, if convergence is met in less than K_d iterations.[8]

Appendix 3: Second-order temporal discretization

Discretization of temporally second-order equations can be illustrated by considering

$$\ddot{\boldsymbol{U}} = \dot{\boldsymbol{V}} = \boldsymbol{\Psi}(\boldsymbol{U}). \tag{9.1}$$

Expanding the field $\boldsymbol{V}$ in a Taylor series about $t + \phi\Delta t$ we obtain

$$\boldsymbol{V}(t+\Delta t) = \boldsymbol{V}(t+\phi\Delta t) + \frac{d\boldsymbol{V}}{dt}|_{t+\phi\Delta t}(1-\phi)\Delta t + \frac{1}{2}\frac{d^2\boldsymbol{V}}{dt^2}|_{t+\phi\Delta t}(1-\phi)^2(\Delta t)^2 + \mathcal{O}((\Delta t)^3) \tag{9.2}$$

and

$$\boldsymbol{V}(t) = \boldsymbol{V}(t+\phi\Delta t) - \frac{d\boldsymbol{V}}{dt}|_{t+\phi\Delta t}\phi\Delta t + \frac{1}{2}\frac{d^2\boldsymbol{V}}{dt^2}|_{t+\phi\Delta t}\phi^2(\Delta t)^2 + \mathcal{O}((\Delta t)^3) \tag{9.3}$$

Subtracting the two expressions yields

$$\frac{d\boldsymbol{V}}{dt}|_{t+\phi\Delta t} = \frac{\boldsymbol{V}(t+\Delta t) - \boldsymbol{V}(t)}{\Delta t} + \hat{\mathcal{O}}(\Delta t), \tag{9.4}$$

where $\hat{\mathcal{O}}(\Delta t) = \mathcal{O}((\Delta t)^2)$, when $\phi = \frac{1}{2}$. Thus, inserting this into the governing equation yields

$$\boldsymbol{V}(t+\Delta t) = \boldsymbol{V}(t) + \Delta t\boldsymbol{\Psi}(t+\phi\Delta t) + \hat{\mathcal{O}}((\Delta t)^2). \tag{9.5}$$

Note that adding a weighted sum of Eqs. 9.2 and 9.3 yields

$$\boldsymbol{V}(t+\phi\Delta t) = \phi\boldsymbol{V}(t+\Delta t) + (1-\phi)\boldsymbol{V}(t) + \mathcal{O}((\Delta t)^2), \tag{9.6}$$

which will be useful shortly. Now expanding the field $\boldsymbol{U}$ in a Taylor series about $t + \phi\Delta t$ we obtain

$$\boldsymbol{U}(t+\Delta t) = \boldsymbol{U}(t+\phi\Delta t) + \frac{d\boldsymbol{U}}{dt}|_{t+\phi\Delta t}(1-\phi)\Delta t + \frac{1}{2}\frac{d^2\boldsymbol{U}}{dt^2}|_{t+\phi\Delta t}(1-\phi)^2(\Delta t)^2 + \mathcal{O}((\Delta t)^3) \tag{9.7}$$

and

$$\boldsymbol{U}(t) = \boldsymbol{U}(t+\phi\Delta t) - \frac{d\boldsymbol{U}}{dt}|_{t+\phi\Delta t}\phi\Delta t + \frac{1}{2}\frac{d^2\boldsymbol{U}}{dt^2}|_{t+\phi\Delta t}\phi^2(\Delta t)^2 + \mathcal{O}((\Delta t)^3). \tag{9.8}$$

Subtracting the two expressions yields

$$\frac{\boldsymbol{U}(t+\Delta t) - \boldsymbol{U}(t)}{\Delta t} = \boldsymbol{V}(t+\phi\Delta t) + \hat{\mathcal{O}}(\Delta t). \tag{9.9}$$

Inserting Eq. 9.6 yields

$$\boldsymbol{U}(t+\Delta t) = \boldsymbol{U}(t) + (\phi\boldsymbol{V}(t+\Delta t) + (1-\phi)\boldsymbol{V}(t))\,\Delta t + \hat{\mathcal{O}}((\Delta t)^2). \tag{9.10}$$

and thus using Eq. 9.5 yields

$$\boldsymbol{U}(t+\Delta t) = \boldsymbol{U}(t) + \boldsymbol{V}(t)\Delta t + \phi(\Delta t)^2\boldsymbol{\Psi}(\boldsymbol{U}(t+\phi\Delta t)) + \hat{\mathcal{O}}((\Delta t)^2). \tag{9.11}$$

The term $\boldsymbol{\Psi}(\boldsymbol{U}(t+\phi\Delta t))$ can be handled in two main ways:

- $\boldsymbol{\Psi}(t+\phi\Delta t) \approx \boldsymbol{\Psi}(\phi\boldsymbol{U}(t+\Delta t) + (1-\phi)\boldsymbol{U}(t))$ or
- $\boldsymbol{\Psi}(t+\phi\Delta t) \approx \phi\boldsymbol{\Psi}(\boldsymbol{U}(t+\Delta t)) + (1-\phi)\boldsymbol{\Psi}(\boldsymbol{U}(t))$.

The differences are quite minute between either of the above, thus, for brevity, we choose the latter. In summary, we have the following:

$$\boldsymbol{U}(t+\Delta t) = \boldsymbol{U}(t) + \boldsymbol{V}(t)\Delta t + \phi(\Delta t)^2\,(\phi\boldsymbol{\Psi}(\boldsymbol{U}(t+\Delta t)) + (1-\phi)\boldsymbol{\Psi}(\boldsymbol{U}(t))) + \hat{\mathcal{O}}((\Delta t)^2). \tag{9.12}$$

We note that

- When $\phi = 1$, then this is the (implicit) Backward Euler scheme, which is very stable (very dissipative) and $\mathcal{O}((\Delta t)^2)$ locally in time,

[7] Typically, K_d is chosen to be between five to ten iterations.

[8] At the implementation level, since the exact solution is unknown, the following relative error term is used, $\varpi^{L+1,K} \overset{\text{def}}{=} ||\boldsymbol{W}^{L+1,K} - \boldsymbol{W}^{L+1,K-1}||$.

- When $\phi = 0$, then this is the (explicit) Forward Euler scheme, which is conditionally stable and $\mathcal{O}((\Delta t)^2)$ locally in time,
- When $\phi = 0.5$, then this is the (implicit) "Midpoint" scheme, which is stable and $\hat{\mathcal{O}}((\Delta t)^2) = \mathcal{O}((\Delta t)^3)$ locally in time.

In summary, we have for the velocity[9]

$$\begin{aligned} \boldsymbol{V}(t+\Delta t) = \boldsymbol{V}(t) + \Delta t\, (\phi \boldsymbol{\Psi}(\boldsymbol{U}(t+\Delta t)) \\ +(1-\phi)\boldsymbol{\Psi}(\boldsymbol{U}(t))) \end{aligned} \tag{9.13}$$

and for the position

$$\begin{aligned} \boldsymbol{U}(t+\Delta t) &= \boldsymbol{U}(t) + \boldsymbol{V}(t+\phi\Delta t)\Delta t \\ &= \boldsymbol{U}(t) + (\phi \boldsymbol{V}(t+\Delta t) + (1-\phi)\boldsymbol{V}(t))\, \Delta t, \end{aligned} \tag{9.14}$$

or more explicitly

$$\begin{aligned} \boldsymbol{U}(t+\Delta t) = \boldsymbol{U}(t) + \boldsymbol{V}(t)\Delta t + \phi(\Delta t)^2\, (\phi \boldsymbol{\Psi}(\boldsymbol{U}(t+\Delta t)) \\ +(1-\phi)\boldsymbol{\Psi}(\boldsymbol{U}(t)))\,. \end{aligned} \tag{9.15}$$

In iterative (recursion) form

$$\begin{aligned} \boldsymbol{U}^{L+1,K} = & \underbrace{(\phi\Delta t)^2 \boldsymbol{\Psi}(\boldsymbol{U}^{L+1,K-1})}_{\mathcal{G}(\boldsymbol{U}^{L+1,K-1})} \\ & + \underbrace{\boldsymbol{U}^L + \boldsymbol{V}^L \Delta t + (\Delta t)^2 \phi(1-\phi)\boldsymbol{\Psi}(\boldsymbol{U}^L)}_{\mathcal{R}} \end{aligned} \tag{9.16}$$

Remark Applying this scheme to the balance of linear momentum continuum formulation, under infinitesimal deformations, $\nabla_x \cdot \boldsymbol{\sigma} + \boldsymbol{f} = \rho \frac{\partial^2 \boldsymbol{u}}{\partial t^2}$ we use $\boldsymbol{\Psi}(\boldsymbol{u}(t)) = \frac{\nabla_x \cdot \boldsymbol{\sigma} + \boldsymbol{f}}{\rho}$, and must apply the (iterative) process introduced earlier to all nodes in the system.

References

1. Avci B, Wriggers P (2012) A DEM-FEM coupling approach for the direct numerical simulation of 3D particulate flows. J Appl Mech 79:010901-1–010901-7
2. Akisanya AR, Cocks ACF, Fleck NA (1997) The yield behavior of metal powders. Int J Mech Sci 39:1315–1324
3. Ames WF (1977) Numerical methods for partial differential equations, 2nd edn. Academic Press, New York
4. Anand L, Gu C (2000) Granular materials: constitutive equations and shear localization. J Mech Phys Solids 48:1701–1733
5. Axelsson O (1994) Iterative solution methods. Cambridge University Press, Cambridge
6. Bianco M, Bilardi G, Pesavento F, Pucci G, Schrefler BA (2003) A frontal solver tuned for fully coupled non-linear hygro-thermo-mechanical problems. Int J Numer Methods Eng 57:18011818
7. Bolintineanu DS, Grest GS, Lechman JB, Pierce F, Plimpton SJ, Schunk PR (2014) Particle dynamics modeling methods for colloid suspensions. Comput Part Mech 1(3):321–356
8. Brown S, Abou-Chedid G (1994) Yield behavior of metal powder assemblages. J Mech Phys Solids 42:383–398
9. Campello EMB, Zohdi TI (2014) A computational framework for simulation of the delivery of substances into cells. Int J Numer Methods Biomed Eng 30(11):1132–1152
10. Campello EMB, Zohdi TI (2014) Design evaluation of a particle bombardment system to deliver substances into cells. Comput Mech Eng Sci 98(2):221–245
11. Cante J, Davalos C, Hernandez JA, Oliver J, Jonsen P, Gustafsson G, Haggblad HA (2014) PFEM-based modeling of industrial granular flows. Comput Part Mech 1(1):47–70
12. Carbonell JM, Onate E, Suarez B (2010) Modeling of ground excavation with the particle finite element method. J Eng Mech, ASCE 136:455–463
13. Deckard C (1986) Method and apparatus for producing parts by selective sintering US Patent 4,863,538
14. Domas F (1997) Eigenschaft profile und Anwendungsübersicht von EPE und EPP. Technical report of the BASF Company
15. Donev A, Cisse I, Sachs D, Variano EA, Stillinger F, Connelly R, Torquato S, Chaikin P (2004a) Improving the density of jammed disordered packings using ellipsoids. Science 303:990–993
16. Donev A, Stillinger FH, Chaikin PM, Torquato S (2004b) Unusually dense crystal ellipsoid packings. Phys Rev Lett 92:255506
17. Donev A, Torquato S, Stillinger F (2005a) Neighbor list collision-driven molecular dynamics simulation for nonspherical hard particles-I. Algorithmic details. J Comput Phys 202:737
18. Donev A, Torquato S, Stillinger F (2005b) Neighbor list collision-driven molecular dynamics simulation for nonspherical hard particles-II. Application to ellipses and ellipsoids. J Comput Phys 202:765
19. Donev A, Torquato S, Stillinger FH (2005c) Pair correlation function characteristics of nearly jammed disordered and ordered hard-sphere packings. Phys Rev E 71:011105
20. Duran J (1997) Sands, powders and grains. An introduction to the physics of granular matter. Springer, New York
21. Dwivedi G, Wentz T, Sampath S, Nakamura T (2010) Assessing process and coating reliability through monitoring of process and design relevant coating properties. J Thermal Spray Technol 19:695–712
22. Fleck NA (1995) On the cold compaction of powders. J Mech Phys Solids 43:1409–1431
23. Fuller SB, Wilhelm EJ, Jacobson JM (2002) Ink-jet printed nanoparticle microelectromechanical systems. J Microelectromech Syst 11:54–60
24. Gamota D, Brazis P, Kalyanasundaram K, Zhang J (2004) Printed organic and molecular electronics. Kluwer Academic Publishers, New York
25. Gethin DT, Lewis RW, Ransing RS (2003) A discrete deformable element approach for the compaction of powder systems. Model Simul Mater Sci Eng 11(1):101–114
26. Ghosh S (2011) Micromechanical analysis and multi-scale modeling using the Voronoi cell finite element method. CRC Press/Taylor & Francis, Boca Raton
27. Ghosh S, Dimiduk D (2011) Computational methods for microstructure-property relations. Springer, New York
28. Gu C, Kim M, Anand L (2001) Constitutive equations for metal powders: application to powder forming processes. Int J Plast 17:147–209
29. Haruta M (2002) Catalysis of gold nanoparticles deposited on metal oxides. Cattech 6(3):102–115

[9] In order to streamline the notation, we drop the cumbersome $\mathcal{O}(\Delta t)$-type terms.

30. Hashin Z, Shtrikman S (1962) On some variational principles in anisotropic and nonhomogeneous elasticity. J Mech Phys Solids 10:335–342
31. Hashin Z (1983) Analysis of composite materials: a survey. ASME J Appl Mech 50:481–505
32. Housholder R (1979) Molding process. US Patent 4,247,508
33. Hull C (1984) Apparatus for production of three-dimensional objects by stereolithography. US Patent 4,575,330
34. Jikov VV, Kozlov SM, Olenik OA (1994) Homogenization of differential operators and integral functionals. Springer, New York
35. Kachanov LM (1986) Introduction to continuum damage mechanics. Martinus Nijoff, Dordricht
36. Kachanov M (1993) Elastic solids with many cracks and related problems. Advance applied mechanics, vol 30. Academic Press, New York
37. Kachanov M, Tsukrov I, Shafiro B (1994) Effective moduli of solids with cavities of various shapes. Appl Mech Rev 47:S151–S174
38. Kachanov M, Sevostianov I (2005) On the quantitative characterization of microstructures and effective properties. Int J Solids Struct 42:309–336
39. Kansaal A, Torquato S, Stillinger F (2002) Diversity of order & densities in jammed hard-particle packings. Phys Rev E 66:041109
40. Martin P (2009) Handbook of deposition technologies for films and coatings, 3rd edn. Elsevier, Oxford
41. Martin P (2011) Introduction to surface engineering and functionally engineered materials. Scrivener and Elsevier, Hoboken
42. Labra C, Onate E (2009) High-density sphere packing for discrete element method simulations. Commun Numer Methods Eng 25(7):837–849
43. Leonardi A, Wittel FK, Mendoza M, Herrmann HJ (2014) Coupled DEM-LBM method for the free-surface simulation of heterogeneous suspensions. Comput Part Mech 1(1):3–13
44. Lewis RW, Gethin DT, Yang XSS, Rowe RC (2005) A combined finite-discrete element method for simulating pharmaceutical powder tableting. Int J Numer Methods Eng 62:853869
45. Lewis RW, Schrefler BA, Simoni L (1992) Coupling versus uncoupling in soil consolidation. Int J Numer Anal Methods Geomech 15:533–548
46. Lewis RW, Schrefler BA (1998) The finite element method in the static and dynamic deformation and consolidation of porous media, 2nd edn. Wiley press, New York
47. Liu Y, Nakamura T, Dwivedi G, Valarezo A, Sampath S (2008) Anelastic behavior of plasma sprayed zirconia coatings. J Am Ceram Soc 91:4036–4043
48. Liu Y, Nakamura T, Srinivasan V, Vaidya A, Gouldstone A, Sampath S (2007) Nonlinear elastic properties of plasma sprayed zirconia coatings and associated relationships to processing conditions. Acta Mater 55:4667–4678
49. Maxwell JC (1867) On the dynamical theory of gases. Philos Trans Soc Lond 157:49
50. Maxwell JC (1873) A treatise on electricity and magnetism, 3rd edn. Clarendon Press, Oxford
51. Mura T (1993) Micromechanics of defects in solids, 2nd edn. Kluwer Academic Publishers, Dordrecht
52. Nakamura T, Liu Y (2007) Determination of nonlinear properties of thermal sprayed ceramic coatings via inverse analysis. Int J Solids Struct 44:1990–2009
53. Nakamura T, Qian G, Berndt CC (2000) Effects of pores on mechanical properties of plasma sprayed ceramic coatings. J Am Ceram Soc 83:578–584
54. Nakanishi H, Bishop KJM, Kowalczyk B, Nitzan A, Weiss EA, Tretiakov KV, Apodaca MM, Klajn R, Stoddart JF, Grzybowski BA (2009) Photoconductance and inverse photoconductance in thin films of functionalized metal nanoparticles. Nature 460:371–375
55. Nemat-Nasser S, Hori M (1999) Micromechanics: overall properties of heterogeneous solids, 2nd edn. Elsevier, Amsterdam
56. Onate E, Idelsohn SR, Celigueta MA, Rossi R (2008) Advances in the particle finite element method for the analysis of fluid-multibody interaction and bed erosion in free surface flows. Comput Methods Appl Mech Eng 197(19–20):1777–1800
57. Onate E, Celigueta MA, Idelsohn SR, Salazar F, Surez B (2011) Possibilities of the particle finite element method for fluid-soil-structure interaction problems. Comput Mech 48:307–318
58. Pöschel T, Schwager T (2004) Computational granular dynamics. Springer, New York
59. Qian G, Nakamura T, Berndt CC (1998) Effects of thermal gradient and residual stresses on thermal barrier coating fracture. Mech Mater 27:91–110
60. Ransing RS, Lewis RW, Gethin DT (2004) Using a deformable discrete-element technique to model the compaction behaviour of mixed ductile and brittle particulate systems. Philos Trans R Soc Ser A 362(1822):1867–1884
61. Rayleigh JW (1892) On the influence of obstacles arranged in rectangular order upon properties of a medium. Philos Mag 32:481–491
62. Rojek J, Labra C, Su O, Onate E (2012) Comparative study of different discrete element models and evaluation of equivalent micromechanical parameters. Int J Solids Struct 49:1497–1517. doi:10.1016/j.ijsolstr.2012.02.032
63. Rojek J (2014) Discrete element thermomechanical modelling of rock cutting with valuation of tool wear. Comput Part Mech 1(1):71–84
64. Onate E, Celigueta MA, Latorre S, Casas G, Rossi R, Rojek J (2014) Lagrangian analysis of multiscale particulate flows with the particle finite element method. Comput Part Mech 1(1):85–102
65. Schrefler BA (1985) A partitioned solution procedure for geothermal reservoir analysis. Commun Appl Numer Methods 1:53–56
66. Sevostianov I, Gorbatikh L, Kachanov M (2001) Recovery of information of porous/microcracked materials from the effective elastic/conductive properties. Mater Sci Eng A 318:1–14
67. Sevostianov I, Kachanov M (2008) Connections between elastic and conductive properties of heterogeneous materials. Adv Appl Mech 42:69–253
68. Sevostianov I, Kachanov M (2000) Modeling of the anisotropic elastic properties of plasma-sprayed coatings in relation to their microstructure. Acta Mater 48(6):1361–1370
69. Sevostianov I, Kachanov M (2001) Thermal conductivity of plasma sprayed coatings in relation to their microstructure. J Therm Spray Technol 9(4):478–482
70. Sevostianov I, Kachanov M (2001) Plasma-sprayed ceramic coatings: anisotropic elastic and conductive properties in relation to the microstructure; cross-property correlations, with I. Sevostianov. Mater Sci Eng-A 297:235–243
71. Tatzel H (1996) Grundlagen der Verarbeitungstechnik von EPP-Bewährte und neue Verfahren. Technical report of the BASF Company
72. Torquato S (2001) Random heterogeneous materials: microstructure and macroscopic properties. Springer, New York
73. Turska E, Schrefler BA (1994) On consistency, stability and convergence of staggered solution procedures. Rend Mat Acc Lincei, Rome, S. 9, 5:265–271
74. Wang X, Schrefler BA (1998) A multifrontal parallel algorithm for coupled thermo-hydro-mechanical analysis of deforming porous media. Int J Numer Methods Eng 43:1069–1083
75. Widom B (1966) Random sequential addition of hard spheres to a volume. J Chem Phys 44:3888–3894
76. Young DM (1950) Iterative methods for solving partial difference equations of elliptic type. Doctoral thesis. Harvard University

77. Zienkiewicz OC (1984) Coupled problems & their numerical solution. In: Lewis RW, Bettes P, Hinton E (eds) Numerical methods in coupled systems. Wiley, Chichester, pp 35–38
78. Zienkiewicz OC, Paul DK, Chan AHC (1988) Unconditionally stable staggered solution procedure for soil-pore fluid interaction problems. Int J Numer Methods Eng 26:1039–1055
79. Zohdi TI (2002) An adaptive-recursive staggering strategy for simulating multifield coupled processes in microheterogeneous solids. Int J Numer Methods Eng 53:1511–1532
80. Zohdi TI (2003) On the compaction of cohesive hyperelastic granules at finite strains. Proc R Soc 454(2034):1395–1401
81. Zohdi TI (2003) Genetic design of solids possessing a random-particulate microstructure. Philos Trans R Soc 361(1806):1021–1043
82. Zohdi TI (2004) Modeling and simulation of a class of coupled thermo-chemo-mechanical processes in multiphase solids. Comput Methods Appl Mech Eng 193(6–8):679–699
83. Zohdi TI (2006) Computation of the coupled thermo-optical scattering properties of random particulate systems. Comput Methods Appl Mech Eng 195:5813–5830
84. Zohdi TI, Wriggers P (2008) Introduction to computational micromechanics. Springer, New York Second Reprinting
85. Zohdi TI (2010) Simulation of coupled microscale multiphysical-fields in particulate-doped dielectrics with staggered adaptive FDTD. Comput Methods Appl Mech Eng 199:79–101
86. Zohdi TI (2012) Dynamics of charged particulate systems. Modeling, theory and computation. Springer, New York
87. Zohdi TI (2012) Electromagnetic properties of multiphase dielectrics. A primer on modeling, theory and computation. Springer, New York
88. Zohdi TI (2013a) Numerical simulation of charged particulate cluster-droplet impact on electrified surfaces. J Comput Phys 233:509–526
89. Zohdi TI (2013b) Rapid simulation of laser processing of discrete particulate materials. Arch Comput Methods Eng. doi:10.1007/s11831-013-9092-6 pp 1–17
90. Zohdi TI (2014) A direct particle-based computational framework for electrically-enhanced thermo-mechanical sintering of powdered materials. Math Mech Solids. doi:10.1007/s11831-013-9092-6 pp 1–21
91. Zohdi T (2014) Embedded electromagnetically sensitive particle motion in functionalized fluids. Comput Part Mech 1(1):27–45
92. Zohdi TI (2014) Additive particle deposition and selective laser processing-a computational manufacturing framework. Comput Mech 54:171–191